

Heralding pure single photons: a comparison between counter-propagating and co-propagating twin photons

Alessandra Gatti^{1,2} and Enrico Brambilla²

¹ *Istituto di Fotonica e Nanotecnologie del CNR, Piazza Leonardo Da Vinci 32, Milano, Italy;* ² *Dipartimento di Scienza e Alta Tecnologia dell'Università dell'Insubria, Via Valleggio 11, Como, Italy**

We investigate different strategies suitable to generate pure heralded single photons through spontaneous parametric down-conversion, comparing the counter-propagating geometry studied in [1] with more conventional co-propagating configurations which enhance the purity of the heralded photon state through the technique of group-velocity matching. Our analysis is based on the correlation of twin photons in the temporal domain, a non-standard approach that provides a physical view of the mechanisms that permit to eliminate the temporal entanglement of the state and to generate high-purity heralded photons. The Schmidt number associated to the temporal modes, which provides a more quantitative estimate of the purity, is then calculated. The efficiency of the various strategies and the individual properties of the heralded photons thereby generated are also compared.

PACS numbers: 42.65.Lm, 42.50.Ar, 42.50.Dv

arXiv:1706.01790v1 [quant-ph] 6 Jun 2017

* Alessandra.Gatti@mi.infn.it

INTRODUCTION

Single-photon states are of outstanding interest in modern quantum optics, as the basis of fundamental tests of quantum mechanics and of a variety of quantum technologies (see e.g. [2, 3] for recent surveys of single-photon techniques and applications). In order to generate truly single photons, one of the most efficient method is based on a conditional measurement, where a two-photon state is generated and the presence of a single photon is *heralded* by detection of its partner. To this end, parametric processes such as spontaneous parametric down-conversion (PDC) or four-wave mixing (FWM), where one or two photons belonging to a high energy pump laser are occasionally converted into pairs of photons, are routinely employed. The conservation laws ruling these microscopic processes originate a quantum correlation in the spatial and temporal degrees of freedom of the pair, which typically extends over broad spectral and angular bandwidths. Such a high dimensional entanglement may represent a resource for broadband quantum communication or quantum metrology, but is detrimental for the purity of heralded single photons, because detection of the trigger photon projects the state of its twin in a highly mixed state. This represents a limitation for quantum communication/information protocols where single photons are required to be in indistinguishable and capable of high-visibility interference.

The recent development of waveguided PDC (see [4] and reference therein) and of FWM in single-mode fibers [5] opened the possibility to control the spatial degrees of freedom, and to generate the twin photons into a single of few spatial modes. In order to eliminate also the spectro-temporal correlation, a possibility is filtering hard enough that a single spectral mode is selected, but clearly the efficiency of the source is reduced. In order to achieve pure heralded photons with high fluxes, therefore, considerable effort has been devoted to find alternative techniques, which directly reduce the degree of entanglement of the source in order to produce uncorrelated twin photons[6–14]. In such a way a conditional measurement projects the field in a pure single-photon state rather than in a mixed state. In the standard co-propagating geometry (Fig.1b) this task requires careful techniques of group velocity matching, which can be implemented only in some materials and tuning conditions[6, 9].

In recent years, the counter-propagating configuration of PDC, where twin photons are emitted along opposite directions (Fig.1a), emerged as a promising source of heralded pure single photons without the need of group-velocity matching [1, 15]. Proposed by Harris in the sixties [16] and implemented in 2007 by Canalias et al. [17], this config-

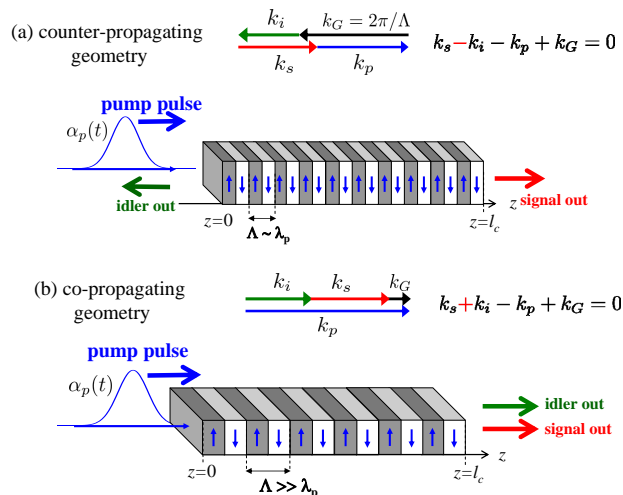


FIG. 1. (a) Scheme of twin-photon generation in the (a) counter-propagating and (b) co-propagating geometries. In the case (a) quasi-phasematching at first order requires submicrometer poling periods $\Lambda \sim \lambda_p$ of the nonlinear material .

uration presents the challenge of requiring a very short poling of the nonlinear material[18, 19]. On the other hand, counter-propagating twin photons and twin beams possess peculiar and attractive features, such as their narrowband character [1, 20–22] and the potentiality to generate in the high-gain regime a robust continuous-variable entanglement [23]. In the spontaneous regime, twin-photons may be naturally generated in either spectrally entangled or decorrelated states by simply modifying the pump pulse duration (or crystal length), without the need of special tuning conditions [1]. Similar features have recently been described in counterpropagating FWM [24].

In this work we focus on the PDC process, and on the temporal correlation of twin photons thereby generated, making a parallel analysis of the two co-propagating and counterpropagating geometries (Fig.1) as sources of heralded single photons. By a systematic comparison of the two configurations, we aim at providing a deeper understanding of the physical mechanisms under which temporal correlation emerges and can eventually be eliminated, which may

turn useful to optimize the existing configurations and to design new ones. Event though our analysis is restricted to the PDC process, some of our results may qualitatively hold also for FWM.

A large part of our analysis will be based on the correlation of twin-photons in the temporal domain. This approach is not standard in the literature[6–15], which mostly focused on their spectral correlation, and provides, in our opinion, a more direct physical view. For example, it will show that the temporal correlation between twin photons can be eliminated only creating conditions such that the timing provided by the pump pulse is more precise than that offered by detecting any of the twin photons. In this way, detection of one photon does not give any better information on the exit time of its twin than by not detecting it, and the two-photon state appears uncorrelated.

From a more quantitative point of view, we will derive an approximated formula for the Schmidt number, to our knowledge not present in the former literature, which holds for both geometries and gives a simple means for evaluating the degree of purity of the heralded photon based only on two parameters, that describe the characteristic time scales of the source.

Finally, the individual spectro-temporal properties of the heralded photons, which are of great importance in view of different applications will be investigated in parallel. In particular, we will see that either narrowband or broadband pure heralded photons are characteristic of the two geometries, and that different strategies of group-velocity matching lead to very different efficiencies of pair production.

The paper is organized as follows: After introducing in Sec.I the two geometries and their different phase-matching conditions, the core of our results is contained in sections II-V. Sec.II describes the temporal correlation of twin photons, in terms both of general formulas valid for any configuration of PDC, and of numerical calculations for specific examples. Sections III calculates the Schmidt number of entanglement. General analytic results obtained within the Gaussian approximation for the biphoton amplitude are compared with more exact numerical ones. Sec IV offers a physical interpretation of the results obtained, while the final Sec.V describes the spectro-temporal properties of heralded photons and compares the efficiency of heralding within the different strategies investigated.

I. COUNTER-PROPAGATING AND CO-PROPAGATING GEOMETRIES

As in most of the previous literature, our analysis is restricted to the purely temporal domain, assuming either a single-mode waveguided configuration, or that a small angular bandwidth is collected.

In the counter-propagating geometry shown in Fig.1a, a coherent pump pulse of central frequency ω_p and temporal profile $\alpha_p(t)$ impinges a nonlinear $\chi^{(2)}$ crystal of length l_c from the left face, and generates counter-propagating photon pairs with, say, the idler photon backpropagating towards the laser source. For the counter-propagating three-wave interaction, momentum conservation requires quasi-phase matching in a periodically poled structure, with a short poling period Λ , such that the momentum associated to the nonlinear grating of the nonlinearity $k_G = \frac{2\pi m}{\Lambda}$, $m = \pm 1, \pm 3 \dots$, approximately compensates the momentum of the pump photon. At first order, it requires Λ on the same order as the pump wavelength in the medium. The central frequencies of the emitted signal and idler fields, ω_s and $\omega_i = \omega_p - \omega_s$, are thus determined by the poling period Λ and the pump central frequency ω_p according to

$$k_s - k_i = k_p - k_G \quad \text{(a) counter-propagating case} \quad (1)$$

where $k_j = \frac{\omega_j}{c} n_j(\omega_j)$, $j = s, i, p$ are the wave-numbers at the corresponding central frequencies ω_j .

In the co-propagating geometry (Fig.1b) all the three fields propagate along the positive z direction. In this case momentum conservation requires

$$k_s + k_i = k_p - k_G \quad \text{(b) co-propagating case} \quad (2)$$

which describes both the case of a bulk crystal, in which $k_G = 0$, or quasi-phasematching in periodically poled structures.

The efficiency of the down-conversion process is described by a dimensionless gain parameter g , proportional to the peak amplitude of the pump laser, the crystal length and the nonlinear susceptibility. Considering the spontaneous regime where $g \ll 1$, and retaining terms at most linear in $g \ll 1$, the signal-idler state at the crystal output takes the well-known form

$$|\phi\rangle = |0\rangle + |\phi_2\rangle \quad (3)$$

$$|\phi_2\rangle = \int d\Omega_s d\Omega_i \psi(\Omega_s, \Omega_i) \hat{a}_s^\dagger(\Omega_s) \hat{a}_i^\dagger(\Omega_i) |0\rangle, \quad (4)$$

corresponding to the superposition of the vacuum and the two-photon state $|\phi_2\rangle$ (see e.g. [1] for a derivation from the more powerful quantum-field description). Here $\hat{a}_s^\dagger(\Omega_s)$ and $\hat{a}_i^\dagger(\Omega_i)$ are signal and idler photon creation operators

in the frequency domain, Ω_j being the offset from the reference frequency ω_j , and

$$\psi(\Omega_s, \Omega_i) = \frac{g}{\sqrt{2\pi}} \tilde{\alpha}_p(\Omega_s + \Omega_i) \text{sinc} \left[\frac{\mathcal{D}^\pm(\Omega_s, \Omega_i) l_c}{2} \right] e^{i\beta(\Omega_s, \Omega_i)} \quad (5)$$

is the so-called spectral biphoton amplitude, giving the joint probability amplitude of detecting a signal photon at frequency $\omega_s + \Omega_s$ and an idler photon at frequency $\omega_i + \Omega_i$. In formula (5)

$$\tilde{\alpha}_p(\Omega) = \int \frac{dt}{\sqrt{2\pi}} e^{i\Omega t} \alpha_p(t); \quad (6)$$

is the spectral amplitude of the pump pulse, where the temporal profile $\alpha_p(t)$ is normalized to its peak value; $\mathcal{D}^\pm(\Omega_s, \Omega_i) l_c$ is the phase-mismatch function, where here and in the following the index + and - refer to the counter-propagating and co-propagating geometries (a) and (b), respectively

$$\mathcal{D}^\pm(\Omega_s, \Omega_i) = \begin{cases} k_p(\Omega_s + \Omega_i) - k_s(\Omega_s) + k_i(\Omega_i) - k_G & \text{(a)} \\ k_p(\Omega_s + \Omega_i) - k_s(\Omega_s) - k_i(\Omega_i) - k_G & \text{(b)} \end{cases} \quad (7)$$

Finally

$$\beta(\Omega_s, \Omega_i) = \frac{l_c}{2} [k_s(\Omega_s) + k_i(\Omega_i) + k_p(\Omega_s + \Omega_i)] \quad (8)$$

is a global phase, acquired during the propagation along the crystal in the absence of any nonlinear effect by a pair of photons generated at the crystal center $z = l_c/2$.

As described in [1, 22, 23], the different sign in front of the idler wave-number $k_i(\Omega_i)$ in Eq. (7) is at the origin of the radically different properties of the two geometries of PDC. This is best seen by expanding the phase mismatch (7) at first order around the reference frequencies (corresponding to $\Omega_j = 0$),

$$\begin{aligned} \mathcal{D}^\pm(\Omega_s, \Omega_i) \frac{l_c}{2} &\approx \frac{l_c}{2} [(k'_p \pm k'_i) \Omega_i + (k'_p - k'_s) \Omega_s] \\ &\equiv \tau_i^\pm \Omega_i + \tau_s \Omega_s, \end{aligned} \quad (9)$$

where $k'_j \equiv v_{gj}^{-1} = \left(\frac{dk_j}{d\Omega_j} \right)_{\Omega_j=0}$ is the inverse group velocity of wave j and we introduced the characteristic times

$$\tau_s = \frac{1}{2} \left(\frac{l_c}{v_{gp}} - \frac{l_c}{v_{gs}} \right) \quad (10)$$

$$\tau_i^\pm = \frac{1}{2} \left(\frac{l_c}{v_{gp}} \pm \frac{l_c}{v_{gi}} \right) \quad (11)$$

which involve either the difference or the sum of the group velocities of the pump and the down-converted field, depending whether the latter co-propagates or counterpropagates with respect to the former, or, in other words, they involve the *relative* group velocities of the down-converted photons with respect to the pump. These constants represent the characteristic temporal separations between the centers of the pump and down-converted wave-packets, and describe how much delayed from the pump a pair of twin photons generated at the crystal center arrive at their end faces. In the co-propagating case τ_s and τ_i^- are both determined by the group velocity mismatch (GVM) with respect to the pump, and are typically on the same order of magnitude, unless some particular strategy of group velocity matching is employed. By contrast, in the counter-propagating case, the time constant associated to the backward photon τ_i^+ involves the group velocities sum (GVS) and is on the order of the photon transit time across the crystal, which exceeds the GVM time by one or two orders of magnitude.

As will be clear in the following (see also [1, 6, 7, 25]), the possibility to generate heralded photons with a high degree of purity depends on the relative sizes and signs of these time constants, and on how they compare to the pump duration T_p . Therefore we introduce the ratio

$$\eta = \frac{\tau_s}{\tau_i^\pm}, \quad (12)$$

which can be positive or negative (only τ_i^+ is always positive, while τ_s and τ_i^- can be either positive or negative). Clearly, in the counter-propagating case

$$|\eta| = \frac{|k'_p - k'_s|}{k'_p + k'_i} = \frac{|\tau_s|}{\tau_i^+} \ll 1 \quad (13)$$

for any choice of materials and phase matching conditions. Without loss of generality, we assume that in the co-propagating case the signal and idler are chosen so that $|\tau_s| \leq |\tau_i^-|$, so that in both configurations

$$-1 \leq \eta \leq 1 \quad (14)$$

An analogous linear approximation of the global phase appearing in Eq.(5) gives:

$$\begin{aligned} \beta(\Omega_s, \Omega_i) &\approx \frac{l_c}{2} [k_s + k_i + k_p + (k'_s + k'_p)\Omega_s + (k'_i + k'_p)\Omega_i] \\ &= \text{const.} + t_{As}\Omega_s + t_{Ai}\Omega_i, \end{aligned} \quad (15)$$

where

$$t_{As} = \frac{l_c}{2v_{gs}} + \frac{l_c}{2v_{gp}} = t_{Ap} - \tau_s \quad (16a)$$

$$t_{Ai} = \frac{l_c}{2v_{gi}} + \frac{l_c}{2v_{gp}} = t_{Ap} - \tau_i^- \quad (16b)$$

can be considered as the times at which two twin photons downconverted from the pump peak at $z = l_c/2$ - pictured as wave-packets propagating without deformation - arrive at their respective end faces of the crystal. They represent the exit time of the centers of the signal and idler wavepackets, assuming that at $t = 0$ the center of the pump pulse enters the crystal ($t_{Ap} = \frac{l_c}{v_{gp}}$ is then the exit time of the pump) .

We notice that the omission of second and higher order terms in Eqs. (9) and (15) is valid only for small bandwidths, and corresponds to neglecting the temporal dispersion. This is well justified in the counter-propagating configuration, which involves narrow down-conversion spectra [1, 17, 22], while it is less justified in the co-propagating case, because of the larger bandwidths in play. In particular, it is not justified when $\tau_s \simeq \tau_i^-$ (e.g. for type I PDC close to degeneracy).

II. TIME-DOMAIN VIEW: THE TEMPORAL CORRELATION OF TWIN PHOTONS

An alternative and perhaps more intuitive view of the problem is offered by the joint amplitude in the temporal domain, which is obtained by back-Fourier transforming the joint spectral amplitude

$$\phi(t_s, t_i) = \int \frac{d\Omega_s}{\sqrt{2\pi}} \int \frac{d\Omega_i}{\sqrt{2\pi}} e^{-i(\Omega_s t_s + \Omega_i t_i)} \psi(\Omega_s, \Omega_i) \quad (17)$$

In terms of this function, the two-photon state (4) becomes

$$|\phi_2\rangle = \int dt_s dt_i \phi(t_s, t_i) \hat{a}_s^\dagger(t_s) \hat{a}_i^\dagger(t_i) |0\rangle, \quad (18)$$

where $\hat{a}_s^\dagger(t_s)$, $\hat{a}_i^\dagger(t_i)$ are photon creation operators in the time domain, and for example $\hat{a}_s^\dagger(t_s)|0\rangle \equiv |t_s\rangle$ represents the state with exactly one signal photon at time t_s at the crystal output face. Thus, $\phi(t_s, t_i)$, which was extensively analysed in [1] in the counter-propagating case, represents the joint probability amplitude that a signal and an idler photon exit the crystal slab at times t_s and t_i , respectively, and describes the temporal correlation between the twin photons. The rate of coincidence counts at the crystal exit faces is then given by

$$G_{si}^{(2)}(t_s, t_i) \equiv \langle \hat{a}_s^\dagger(t_s) \hat{a}_s(t_s) \hat{a}_i^\dagger(t_i) \hat{a}_i(t_i) \rangle \approx |\phi(t_s, t_i)|^2. \quad (19)$$

Several plots of this correlation function are shown in Fig.2, where the three columns correspond to three examples chosen as representatives of the two geometries (see Table I for parameters, and Appendix A for details), namely **(i)** a generic counter-propagating configuration, not specifically optimized for separability, where $\eta \simeq 0.01$, and two co-propagating configurations optimized for separability, with **(ii)** $\eta = 0$, and **(iii)** $\eta = -1$. Condition (ii) is referred to as *asymmetric group-velocity matching* and requires that the signal photon propagates with the same group velocity as the pump ($\tau_s = 0$) [7, 8]. Condition (iii) corresponds to the *symmetric group-velocity matching*, and can be realized only in the co-propagating case, requiring $\tau_s = -\tau_i^+$ [6, 7]. They are usually difficult to satisfy in the visible range, but can be achieved in some $\chi^{(2)}$ material in the near infrared and at telecom wavelengths [3, 6–9]. Experimental evidence of frequency decorrelated photon pairs through this technique were first reported in [8].

crystal	l_c (mm)	phase matching (θ_p)	λ_p	λ_s	λ_i	τ_s	τ_i^\pm	T_p^{min}	η
(i) PPKTP	10mm	type 0 e-ee (90°)	821.4nm	1141nm	2932nm	0.67ps	63ps	4.05ps	0.01
(ii) KDP	10mm	type II e-oe (67.8°)	415nm	830nm	830nm	0	0.72ps	0	0
(iii) BBO	10mm	type II e-oe (28.8°)	757nm	1514nm	1514nm	-0.237ps	0.237ps	0.147ps	-1

TABLE I. Phase-matching conditions and characteristic time constants for the three crystals taken as examples: (i) periodically poled KTP, with 800nm poling period for the counter-propagating configuration, (ii) KDP and (iii) BBO bulk crystal for the two co-propagating configurations.

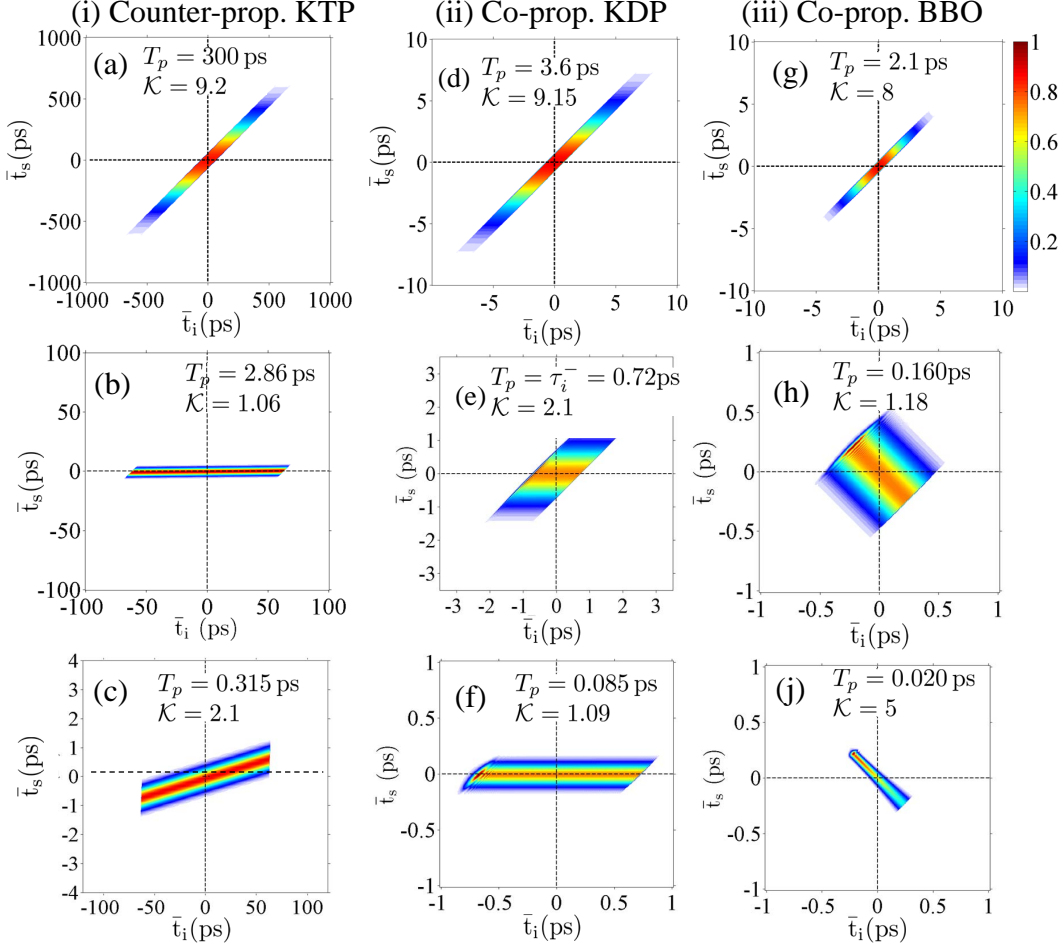


FIG. 2. Temporal correlation $|\phi(\bar{t}_s, \bar{t}_i)|^2$, representing the joint probability of finding a signal and an idler twin photons at times $t_s = \bar{t}_s + t_{As}$ and $t_i = \bar{t}_s + t_{Ai}$ at their crystal exit faces, where t_{Aj} are the reference times defined by Eq.(16). In each panel \mathcal{K} shows the Schmidt number of entanglement (see next section), with $\mathcal{K} = 1$ corresponding to perfect separability. In each column the pump duration T_p decreases from top to bottom, and panels (b), (f), (h) correspond to the minima of \mathcal{K} in Fig.4, and represent the most separable conditions for each example

The plots in Fig.2 have been calculated from Eq.(17) without resorting to any approximation, by using the complete Sellmeier dispersion formula in [26–28] for evaluating the wave-numbers. If the linear approximations (9) and (15) are instead employed, the Fourier transform (17) can be explicitly calculated [1], obtaining

$$\phi(\bar{t}_s, \bar{t}_i) = \frac{g}{2|\tau_i^\pm - \tau_s|} \alpha_p \left(\frac{\bar{t}_s - \eta \bar{t}_i}{1 - \eta} \right) \text{Rect} \left(\frac{\bar{t}_s - \bar{t}_i}{|\tau_i^\pm - \tau_s|} \right) \quad (20)$$

where constant phase factors have been omitted. The barred arguments

$$\bar{t}_j = t_j - t_{Aj} \quad j = s, i, \quad (21)$$

are the exit times of the twin photons measured relative to the central exit times t_{Aj} of their wavepackets, [see Eq. (16)]. The temporal correlation in Eq.(20) is the product of two factors: the first one is the pump temporal profile $\alpha_p(t)$, that we can e.g. take as a Gaussian, the second one is the box function

$$\text{Rect}\left(\frac{t}{\Delta\tau}\right) = \begin{cases} 1 & \text{for } t \in [-\Delta\tau, \Delta\tau] \\ 0 & \text{elsewhere} \end{cases} \quad (22)$$

of width $2\Delta\tau$ and unitary height, where

$$\Delta\tau := |\tau_i^\pm - \tau_s| = \frac{l_c}{2} \left| \frac{1}{v_{gs}} \pm \frac{1}{v_{gi}} \right| \quad (23)$$

represents the typical delay intercurring between the exit times of two twin photons.

The result (20) relies merely on linearization of the propagation phases, and as such fails to be valid for $\tau_s \rightarrow \tau_i^\pm$, when the first order of the Taylor expansion of \mathcal{D}^\pm vanishes. It coincides with the expression analysed in [1], where it was shown that in the counter-propagating configuration the temporal correlation (20) reduces to a factorable function of \bar{t}_s, \bar{t}_i for a range of pump durations intermediate between the two characteristic time scales: $|\tau_i^\pm| \gg T_p \gg |\tau_s|$. The analysis in [1] can then be generalized to a generic geometry.

From a geometric/mathematic viewpoint, we have the noticeable asymptotic behaviors of the temporal correlation in Eq.(20) :

1)Limit of a long pump pulse $T_p \gg |\tau_i^\pm| \geq |\tau_s|$. When the pump pulse is much longer than both characteristic time scales, the pump profile has a slow variation with respect to the much narrower box function. Therefore we can put $\bar{t}_s = \bar{t}_i$ inside the term $\alpha_p\left(\frac{\bar{t}_s - \eta\bar{t}_i}{1-\eta}\right)$, and

$$\phi(\bar{t}_s, \bar{t}_i) \xrightarrow{T_p \gg |\tau_i^\pm|} \frac{g}{2|\tau_i^\pm - \tau_s|} \alpha_p(\bar{t}_s) \text{Rect}\left(\frac{\bar{t}_s - \bar{t}_i}{|\tau_i^\pm - \tau_s|}\right) \quad (24)$$

This formula well reproduces the three upper plots in Fig.2, which exhibit a sharp maximum of the temporal correlation along the diagonal $\bar{t}_s = \bar{t}_i$, expressing the fact that twin photons can be generated at any time along the pump pulse, but they tends to exit almost simultaneously from the crystal (a part from the fixed offset $t_{As} - t_{Ai}$) with a flat distribution of their mutual time delay in the interval $[-\Delta\tau, \Delta\tau]$. This situation corresponds to a joint temporal amplitude not factorable in its arguments, and the two-photon state (18) is entangled.

2)Limit of an ultrashort pump pulse $T_p \ll |\tau_s| \leq |\tau_i^\pm|$. In the opposite limit, the narrow pump profile forces $\bar{t}_s = \eta\bar{t}_i$ inside the box function, and

$$\phi(\bar{t}_s, \bar{t}_i) \xrightarrow{T_p \ll |\tau_s|} \frac{g}{2|\tau_i^\pm - \tau_s|} \alpha_p\left(\frac{\bar{t}_s - \eta\bar{t}_i}{1-\eta}\right) \text{Rect}\left[\frac{\bar{t}_s}{\tau_s}\right] \quad (25)$$

Eq.(25) approximately describes the three lower plots of Fig.2, where the correlation function is peaked along the line $\bar{t}_s = \eta\bar{t}_i$. In the example (ii) where $\eta = 0$, this line is parallel to the \bar{t}_i axis, and the joint temporal amplitude is approximately factorable (see Fig.2f), implying that the two-photon state (18) is separable. In the other two examples with $\eta \neq 0$, the state is entangled. Notice the opposite signs of η in panels (c) and (j) of Fig.2, and that in terms of the original time arguments, by using Eq.(16): $\bar{t}_s = \eta\bar{t}_i$ implies $(t_s - t_{Ap}) = \eta(t_i - t_{Ap})$. Thus, in the ultrashort pump regime, the exit times of twin photons are correlated for $\eta > 0$, while they are *anticorrelated* for $\eta < 0$, as a result of the fact that one photon is slower than the pump while the other is faster.

3)Intermediate pump pulses $|\tau_i^\pm| \gg T_p \gg |\tau_s|$. Notice that this limit is well defined in the counterpropagating case, where the two scales are naturally separated, but needs not to exist in the co-propagating case, where it basically requires that one of the two time constant vanishes, e.g. $\tau_s \rightarrow 0$ as in the example (ii). If this limit exists, then

$$\phi(\bar{t}_s, \bar{t}_i) \xrightarrow{|\tau_i^\pm| \gg T_p \gg |\tau_s|} \frac{g}{2|\tau_i^\pm - \tau_s|} \alpha_p(\bar{t}_s) \text{Rect}\left(\frac{\bar{t}_i}{|\tau_i^\pm - \tau_s|}\right) \quad (26)$$

and the biphoton correlation becomes separable in its arguments, as approximately shown in Fig.2(b),(f), implying that two-photon state (18) is separable.

As a final for this section, we notice that despite the fact that the joint temporal probability as a function of (t_i, t_s) changes completely its shape in different pump regimes, when considered only as a function of the time difference $t_i - t_s$, it always retains a box-function shape. This means that if the coincidence count rate (19) at the crystal exit faces is registered only as a function of the delay between the exit times of the twins, no information is gained about

the entanglement or separability of the state. Indeed, if we rewrite the temporal correlation in Eq. (20) as a function of $\delta t = t_i - t_s$, we have

$$\begin{aligned}\phi(t_s, t_s + \delta t) &\propto \alpha_p \left(\bar{t}_s - \frac{\eta}{1-\eta} \delta \bar{t} \right) \text{Rect} \left(\frac{\delta \bar{t}}{\Delta \tau} \right) \\ \phi(t_i - \delta t, t_i) &\propto \alpha_p \left(\bar{t}_i + \frac{1}{1-\eta} \delta \bar{t} \right) \text{Rect} \left(\frac{\delta \bar{t}}{\Delta \tau} \right)\end{aligned}$$

Then, if coincidence counts are measured only as a function of the time delay $t_i - t_s$ between twin photons, without detecting the absolute arrival time of the signal or of the idler,

$$\begin{aligned}\bar{G}_{si}^{(2)}(\delta t) &= \int dt_s |\phi(t_s, t_s + \delta t)|^2 = \int dt_i |\phi(t_i - \delta t, t_i)|^2 \\ &= \frac{\mathcal{N}}{2\Delta\tau} \text{Rect} \left(\frac{\delta \bar{t}}{\Delta \tau} \right).\end{aligned}\quad (27)$$

where $\mathcal{N} = g^2 \frac{\sqrt{\pi} T_p}{2\Delta\tau}$ is the total number of photon pairs (see Sec.V). Therefore the coincidence counts as a function of $t_i - t_s$ always reproduces the flat distribution of time delays characteristic of the spontaneous process, regardless whether the state is temporally entangled or separable.

Section IV will offer an interpretation of these different behaviours of the temporal correlation of twin photons. Before that, we make first a quantitative analysis of the degree of the entanglement of the state.

III. ENTANGLEMENT QUANTIFICATION

The degree of entanglement of the state is here characterized by the Schmidt number [29, 30], which also estimates the number of independent modes participating to the entangled state [31]. It is defined as the inverse of the purity of the state of each separate subsystem

$$\mathcal{K} = \frac{1}{\text{Tr}\{\hat{\rho}_s^2\}} = \frac{1}{\text{Tr}\{\hat{\rho}_i^2\}} \quad (28)$$

where $\hat{\rho}_s, \hat{\rho}_i$ are the reduced density matrix of the signal and idler when the PDC state (3) is conditioned to a photon count. For example for the signal $\hat{\rho}_s = \frac{1}{\langle \phi_2 | \phi_2 \rangle} \text{Tr}_i \{ |\phi_2\rangle \langle \phi_2| \}$. The inverse of the Schmidt number thus straightforwardly gives the degree of purity of the heralded photon state, via a single parameter that can be calculated without resorting to the explicit Schmidt decomposition. Indeed, for a biphoton state of the form (4), the Schmidt number can be expressed through an integral formula [32, 33]

$$\mathcal{K} = \frac{\mathcal{N}^2}{B} \quad (29)$$

where

$$\mathcal{N} = \int d\Omega_s \int d\Omega_i |\psi(\Omega_s, \Omega_i)|^2 \quad (30)$$

is the mean number of signal or idler photons $\langle \hat{N}_s \rangle = \langle \hat{N}_i \rangle$ generated by the pump pulse;

$$B = \int d\Omega_s \int d\Omega'_s \int d\Omega_i \int d\Omega'_i [\psi(\Omega_s, \Omega_i) \psi(\Omega'_s, \Omega'_i) \psi^*(\Omega_s, \Omega'_i) \psi^*(\Omega'_s, \Omega_i)], \quad (31)$$

represents their normally ordered fluctuations (see [1]): $B = \langle : \delta \hat{N}_s^2 : \rangle = \langle : \delta \hat{N}_i^2 : \rangle$.

In this work the Schmidt number \mathcal{K} is calculated in two ways: (i) "exact" results are obtained by numerical integration of Eqs.(29)-(31), where the complete Sellmeier dispersion formula in [26–28] are used; (ii) approximated analytical results are derived within the "Gaussian approximation" of the spectral amplitude extensively used in former studies of co-propagating PDC [6, 7]. This consists in replacing the sinc function in Eq.(5) by a Gaussian of its argument, and then using the linear approximations (9) and (15), obtaining thereby

$$\text{sinc} \frac{\mathcal{D}^\pm(\Omega_s, \Omega_i) l_c}{2} \rightarrow e^{-\gamma \left[\frac{\mathcal{D}^\pm(\Omega_s, \Omega_i) l_c}{2} \right]^2} \approx e^{-\gamma (\tau_s \Omega_s + \tau_i^\pm \Omega_i)^2} \quad (32)$$

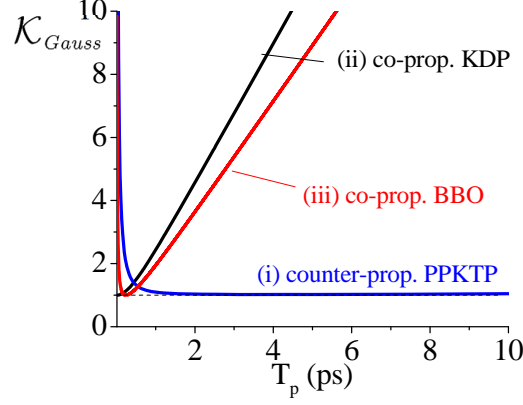


FIG. 3. Schmidt number \mathcal{K} in the Gaussian approximation [Eq.(37)], as a function of the pump duration for (i) counter-propagating PPKTP, (ii) co-propagating KDP $\eta = 0$, (iii) co-propagating BBO $\eta = -1$ (parameters in Table I). In case (i) separability is achieved in a much broader range of pump durations and for longer pulses.

where e.g. $\gamma = 1/6$ if one equates the leading order of the Taylor expansions of the sinc and the Gaussian, or $\gamma = 0.193$ if one requires that they have the same full width at half maximum. In addition, one has to consider a Gaussian pump pulse $\alpha_p(t) = e^{-t^2/2T_p^2}$, of duration T_p and spectral width $\Delta\Omega_p = 1/T_p$, so that $\tilde{\alpha}_p(\Omega) = T_p e^{-\frac{T_p^2}{2}\Omega^2}$, The spectral amplitude (5) takes then the Gaussian form :

$$\psi(\Omega_s, \Omega_i) \rightarrow \frac{gT_p}{\sqrt{2\pi}} e^{i[t_{As}\Omega_s + t_{Ai}\Omega_i]} e^{-\sum_{i,j=s,i} c_{ij}\Omega_i\Omega_j} \quad (33)$$

where constant phase terms have been omitted and the real coefficients c_{ij} [see also [7]] are

$$c_{ss} = \frac{T_p^2}{2} + \gamma\tau_s^2, \quad (34)$$

$$c_{ii} = \frac{T_p^2}{2} + \gamma\tau_i^{\pm 2}, \quad (35)$$

$$c_{is} = \frac{T_p^2}{2} + \gamma\tau_s\tau_i^{\pm}. \quad (36)$$

The approximation (33) allows to extract analytical formula, providing a straightforward comparison between the two cases. Inserting the formula (33) in the expression of \mathcal{K} in Eqs.(29)-(31), and performing the Gaussian integrals involved, we find a single formula that holds for any PDC configuration:

$$\mathcal{K}_{Gauss} = \sqrt{\frac{c_{ss}c_{ii}}{c_{ss}c_{ii} - c_{si}^2}} = \left[1 + \left(1 + \frac{2\gamma\tau_s\tau_i^{\pm}}{T_p^2} \right)^2 \frac{T_p^2}{2\gamma|\tau_i^{\pm} - \tau_s|^2} \right]^{1/2} \quad (37)$$

and gives a simple way of estimating the degree of purity $1/\mathcal{K}$ of heralded single photons for any crystal length and dispersion relations in the medium. We notice that in this formula the various parameters that characterize the PDC process (crystal length, dispersion relations for the three waves) have been condensed in only two parameters, i.e. in the two time constants τ_s and τ_i^{\pm} that rule the relative propagation of the three waves in a crystal of length l_c .

The Gaussian formula (37), seen as a function of the pump duration T_p (see Fig.3), presents for long pump pulses a linear asymptote:

$$\mathcal{K}_{Gauss} \rightarrow \frac{T_p}{\sqrt{2\gamma|\tau_i^{\pm} - \tau_s|}} \quad \text{for } T_p \gg \sqrt{2\gamma|\tau_i^{\pm} - \tau_s|}. \quad (38)$$

corresponding to an entangled state with $\mathcal{K} \gg 1$; by shortening the pump it reaches a minimum, and then it stays close to the curve

$$\mathcal{K}_{Gauss} \rightarrow \frac{\sqrt{2\gamma|\tau_s\tau_i^{\pm}|}}{T_p|\tau_i^{\pm} - \tau_s|} \quad \text{for } T_p \ll \sqrt{2\gamma|\tau_i^{\pm} - \tau_s|} \quad (39)$$

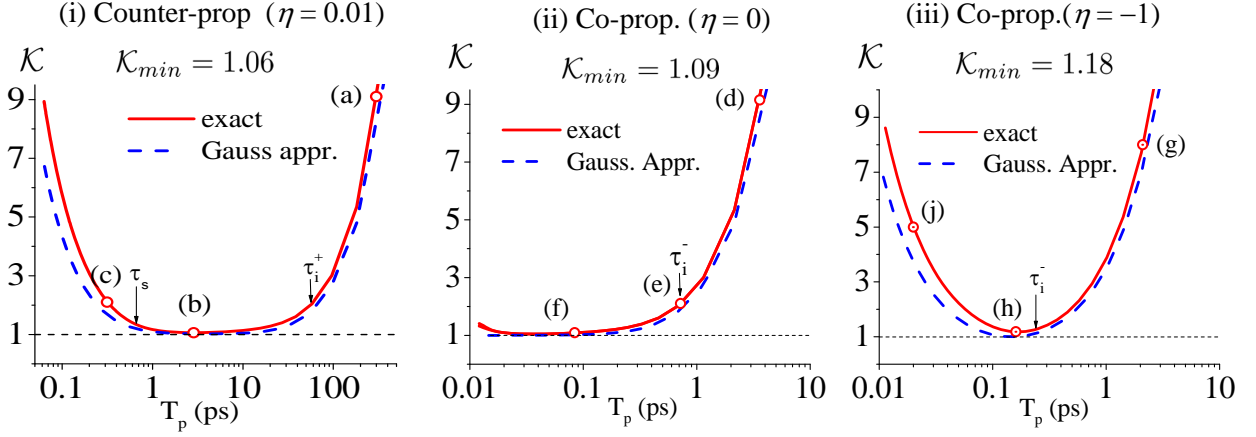


FIG. 4. Schmidt number \mathcal{K} : comparison of the Gaussian result (dashed blue lines) and the exact one (solid red lines) (i) counter-propagating PPKTP, (ii) co-propagating KDP (iii) co-propagating BBO (parameters in Table I). In (i) the state is nearly separable for T_p intermediate between $\tau_s = 0.67\text{ps}$ and $\tau_i^+ = 63\text{ps}$. In (ii) and (iii), separability is achieved only for subpicosecond pulses with $T_p \ll \tau_i^-$. The inverse of \mathcal{K}_{min} is the achievable degree of purity. The hollow red dots correspond to the plots in Figs.2 and 5 .

\mathcal{K}_{Gauss} takes its minimum (the purity takes its maximum) for

$$T_p^{min} = \sqrt{2\gamma|\tau_s\tau_i^\pm|} \quad (40)$$

which is basically the geometrical mean between the two time constants $|\tau_s|$ and $|\tau_i^\pm|$. The minimum value of \mathcal{K} depends both on the sign and on the magnitude of $\eta = \tau_s/\tau_i^\pm$ and is given by

$$\mathcal{K}_{Gauss}^{min} = \begin{cases} 1 & \text{for } \tau_s\tau_i^\pm \leq 0 \rightarrow \eta \leq 0 \\ \frac{\tau_i^\pm + \tau_s}{\tau_i^\pm - \tau_s} = \frac{1+\eta}{1-\eta} & \text{for } \tau_s\tau_i^\pm > 0 \rightarrow \eta > 0 \end{cases} \quad (41)$$

As well known, the Gaussian approximation (33) predicts complete separability $\mathcal{K} = 1$ for $\eta \leq 0$, as can be immediately recognized by inspection of the mixed term c_{is} in Eq. (36). The condition $\eta = 0$, corresponds to the asymmetric group velocity matching of the example (ii), and the ideal value $\mathcal{K} = 1$ is reached only asymptotically for $T_p \rightarrow T_p^{min} = 0$. The condition $\eta < 0$ requires that τ_s and τ_i^\pm have opposite signs (as in the example (II) for $\eta = -1$) and a separable state can be in principle obtained for a finite pump duration $T_p = T_p^{min}$. These conditions straightforwardly lead to a separable Gaussian spectral amplitude (33).

Alternatively, for positive η , the two-photon state can be made almost separable by choosing a configuration for which η is sufficiently small, because

$$\mathcal{K}_{Gauss}^{min} = \frac{1+\eta}{1-\eta} \simeq 1 + 2\eta \quad \text{for } 0 < \eta \ll 1 \quad (42)$$

Notice that this last condition is naturally fulfilled in the counter-propagating case.

Figures 3 and 4 plot the Schmidt number \mathcal{K} as a function of the pump duration, for the three examples described in Table I. Fig.3 superimpose the three results, calculated in the Gaussian approximation (37), while Fig.4 (notice here the horizontal logarithmic scale) shows, for each example, a comparison between the Gaussian result and the exact one, obtained by numerical integration of Eqs.(29)-(31). The Schmidt number curves reproduce in a more quantitative way the behaviour of the temporal correlation analysed in Sec. II (notice that the hollow dots in Fig.4 correspond to the parameters of the plots of in Fig.2): for long pump pulses the state is entangled in all the examples, by shortening the pump pulse \mathcal{K} reaches a minimum close to the ideal value $\mathcal{K}^{min} = 1$ and then it grows again in the two examples with $\eta \neq 0$, while it stays close to the minimum in the example (ii) with $\eta = 0$. However, evident from these figures are the different ranges of pump durations T_p in which separability can be achieved: the counter-propagating case displays a broad plateau with $\mathcal{K} \simeq 1$ for T_p in the range between 2ps and 10ps, while in the co-propagating case separability requires subpicosecond pulses, of duration $T_p \lesssim 100\text{fs} \ll \tau_i^- = 720\text{fs}$ in the $\eta = 0$ case (ii), and $T_p \simeq T_p^{min} = 147\text{fs}$ in the $\eta = -1$ case (iii).

Fig. 4 also shows some discrepancy between the Gaussian results and the exact ones, especially for short pump pulses.

In particular, the minimum of \mathcal{K} is always slightly larger than the Gaussian result (41), and never reaches the ideal value $\mathcal{K} = 1$ even for $\eta \leq 0$. Clearly these discrepancies have to be ascribed both to the replacement of the sinc by a Gaussian and to the effect of dispersion, which becomes relevant only for short pump pulses, and/or long crystal. Because of this, the degree of purity achievable in the counter-propagating configuration with $\eta = 0.01$ is comparable to what obtained in the two cases with $\eta \leq 0$, which require much shorter pump pulses and stringent phase matching conditions.

It is also interesting to see how these results reflect in the shape of the joint spectral probability $|\psi|^2$ in the

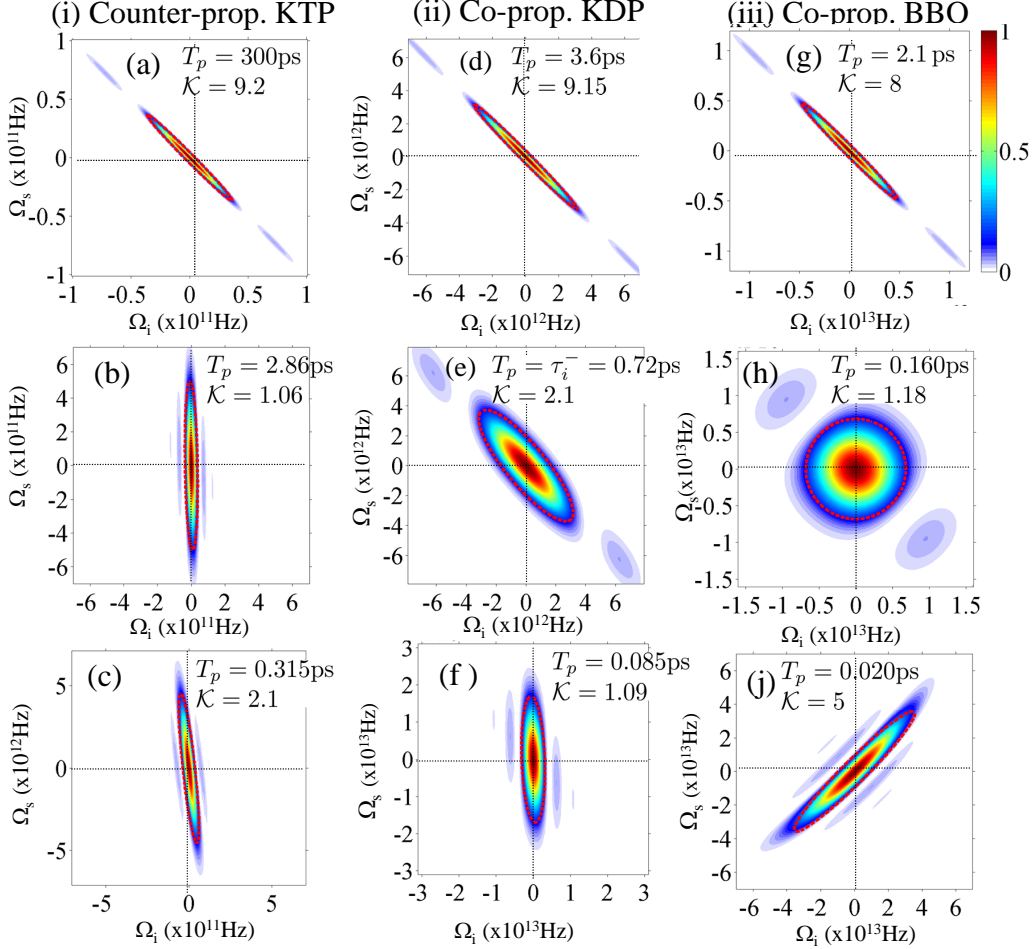


FIG. 5. Joint spectral probability $|\psi(\Omega_s, \Omega_i)|^2$ plotted for pump pulse durations decreasing from top to bottom, for the same parameters in in Fig.2 and in correspondence of the hollow red dots in Fig.4. Panels (b), (f) and (h) represents nearly separable situations. The red ellipses are the isoprobability curves of the Gaussian formula (33). Notice that in panel (c) the idler scale Ω_i is zoomed by a factor 10 with respect to the signal scale.

(Ω_i, Ω_s) plane, plotted in Fig.5 for the same parameters as in Fig. 2. The red ellipses here represent the curves $c_{11}\Omega_s^2 + c_{22}\Omega_i^2 + 2c_{12}\Omega_s\Omega_i = 1$ where according to the Gaussian formula (33) $|\psi|^2$ reduces by $1/e^2$, and permit to estimate visually the validity of the Gaussian approximation. The spectral correlation in this figure gives the complementary view with respect to the temporal correlation in Fig.2, but obviously displays the same amount of entanglement: For long pump pulses (top row) the state is highly entangled in all the three examples, with the biphoton amplitude peaked along the diagonal $\Omega_s = -\Omega_i$ where energy conservation takes place. For short enough pump pulses [bottom panels (c) and (i)] the state is again entangled, with the biphoton amplitude peaked along the line $\Omega_s = -\eta\Omega_i$ where momentum conservation, i.e. phase matching, is realized. Panels (b) (f) and (h) correspond to the optimal conditions for separability, and we see that in these cases the biphoton probability is a nearly factorable function of its arguments, being approximately an ellipse with its principal axes aligned along Ω_s and Ω_i .

IV. INTERPRETATION AND DISCUSSION

In order to understand these behaviors, and to be able to describe the peculiarity of the co-propagating geometry (case $\eta \approx -1$), we resort to the very notion of temporal correlation between the members of a pair, which relies on the possibility of predicting the arrival time of one photon by detecting the arrival time of its twin, with a precision better than what would be obtained with an unconditional measurement.

Referring for definiteness to the signal photon (the one that in any case co-propagates with the pump), we first wonder what is the uncertainty in its arrival time conditioned to detection of the idler. Then we will compare it with the uncertainty in its arrival time not conditioned on the detection of the idler.

There are actually two distinct mechanisms by which the exit time of one photon can be ascertained by detection its twin: one is simply based on their simultaneity, the other relies on the possibility to gain information on the point where down-conversion took place.

The first one prevails for long pump pulses $T_p \gg |\tau_i^\pm| \geq |\tau_s|$. When the duration of the pump pulse is much longer than the delays of twin photons with respect to its center, then the idler and signal wavepackets propagate under the pump pulse, and detection of neither photon gives information on the point of the crystal where the pair was generated. Thus, our ability to infer the arrival time of one photon by detection of its twin is limited by the degree to which they arrive simultaneously at their end faces, i.e. by the spread of the distribution of their mutual time delays. This is described by the box function in Eqs. (20) and (24), characteristic of the spontaneous PDC processes, where a photon pair can be generated at any point along the crystal with uniform probability. Then, depending on the point where down-conversion took place, the delay between the exit of the twins has a flat distribution in the interval $[-\Delta\tau, +\Delta\tau]$ ¹ where $\Delta\tau := \frac{l_c}{2} \left| \frac{1}{v_{gs}} \pm \frac{1}{v_{gi}} \right|$. Notice that counter-propagating photons (+ sign) can be delayed up to their transit time along the sample, since they appear on opposite faces of the crystal. Conversely, co-propagating twins (- sign) exit from the same face, and appear with a small delay ruled by their GVM, the extreme case being when they propagate exactly at the same velocity, and always exit simultaneously, in which case the width of the box function vanishes. According to this mechanism the exit time of the signal can be deduced from that of the idler as

$$\bar{t}_s = \bar{t}_i \quad \text{within } (\delta t_s)_{cond.} \simeq \Delta\tau = |\tau_i^\pm - \tau_s| \quad \text{for } T_p \gg |\tau_i^\pm| \quad (43)$$

where $(\delta t_s)_{cond.}$ indicates the spread of the distribution of the signal arrival time conditioned to detection of the idler, i.e the *correlation time*.

The second mechanism, described by the factor $\alpha_p \left(\frac{\bar{t}_s - \eta \bar{t}_i}{1 - \eta} \right)$ in Eq. (20), prevails for ultrashort pump pulses $T_p \ll |\tau_s| \leq |\tau_i^\pm|$. In this case the twin photons tend to separate from the pump during propagation, and detection of any of them provides an indication of the point where the pair was generated. By using a rough picture of photons as wavepackets propagating without deformation with their group velocities, one can imagine that if a photon pair was generated at a point z_0 , and conversion occurred from a pump photon delayed by δt_p from the centre of the pump pulse, than the idler photon will arrive at its end face at time

$$t_i = \begin{cases} \frac{z_0}{v_{gp}} + \frac{z_0}{v_{gi}} + \delta t_p & \text{counter-prop. case} \\ \frac{z_0}{v_{gp}} + \frac{l_c - z_0}{v_{gi}} + \delta t_p & \text{co-prop. case} \end{cases} \quad (44)$$

i.e, for the barred time argument $\bar{t}_i = t_i - \frac{1}{2} \left(\frac{l_c}{v_{gp}} + \frac{l_c}{v_{gi}} \right)$:

$$\bar{t}_i = \left(z_0 - \frac{l_c}{2} \right) \frac{2}{l_c} \tau_i^\pm + \delta t_p \quad (45)$$

The same argument gives the arrival time of its twin signal photon as

$$\bar{t}_s = \left(z_0 - \frac{l_c}{2} \right) \frac{2}{l_c} \tau_s + \delta t_p \quad (46)$$

where in the above formulas δt_p can be considered as a Gaussian stochastic variable with variance $T_p/\sqrt{2}$, because a pump photon can be downconverted at any time along the pump pulse, with a probability proportional to the Gaussian pump intensity. Then, by comparing Eqs (45) and (46):

$$\bar{t}_s = \bar{t}_i \frac{\tau_s}{\tau_i^\pm} + \delta t_p \left(1 - \frac{\tau_s}{\tau_i^\pm} \right) = \eta \bar{t}_i + (1 - \eta) \delta t_p \quad (47)$$

¹ For the original time arguments, $t_s - t_i = \bar{t}_s - \bar{t}_i + (t_{As} - t_{Ai})$. In the co-propagating case the box function is then shifted to the interval $[0, 2\Delta\tau]$ while in the copropagating case the shift is negligible.

Thus, according to these arguments, the arrival time of the signal conditioned to detection of the idler is

$$\bar{t}_s = \eta \bar{t}_i \quad \text{within } (\delta t_s)_{\text{cond.}} \simeq T_p(1 - \eta) \quad (T_p \ll |\tau_s|) \quad (48)$$

These conditional uncertainties have to be compared with the unconditional uncertainty in the arrival time of the signal, i.e. the spread of the distribution of the exit times of the signal when the idler is not detected. Also here there are two sources of uncertainty, one is the width T_p of the Gaussian distribution of the pump, because the photon can be downconverted from any portion of the pump pulse, the other one is the point of the crystal where down-conversion took place. Depending on the latter, the delay of the signal photon with respect to the center of the pump pulse ranges in the interval $[0, 2|\tau_s|]$ with uniform probability. Clearly, the first mechanism dominates for $T_p \gg |\tau_s|$, as shown by Eqs. (24) and (26), the second mechanism for $T_p \ll |\tau_s|$ [see Eq. (25)]. A more precise analysis, based on the temporal correlation(20) gives

$$(\delta t_s)_{\text{uncond.}} = \sqrt{\frac{T_p^2}{2} + \frac{\tau_s^2}{3}} \rightarrow \begin{cases} \frac{T_p}{\sqrt{2}} & T_p \gg |\tau_s| \\ \frac{|\tau_s|}{\sqrt{3}} & T_p \ll |\tau_s| \end{cases} \quad (49)$$

where $(\delta t_s)_{\text{uncond.}}$ is the variance of the distribution of the arrival times of the signal when the idler is not detected.

Summarizing the results, we have the following situation:

1) For a long pump pulse $T_p \gg |\tau_i^\pm| \geq |\tau_s|$, comparing the unconditional and conditional uncertainties in the arrival time of the signal, in Eqs. (49) and (43), we see that for such long pumps $T_p \gg |\tau_i^\pm|$, the state is in general highly entangled because ².

$$\frac{(\delta t_s)_{\text{uncond.}}}{(\delta t_s)_{\text{cond.}}} \simeq \frac{T_p}{|\tau_i^\pm - \tau_s|} = \frac{T_p}{|\tau_i^\pm|(1 - \eta)} \gg 1 \quad (50)$$

Euristically, the above ratio also gives an estimate of the number of entangled modes, well in accordance with the asymptotic behaviour of the Schmidt number in Eq.(38) for long pump pulses.

2) For an ultrashort pump pulse $T_p \ll |\tau_s| \leq |\tau_i^\pm|$, the state is again highly entangled because

$$\frac{(\delta t_s)_{\text{uncond.}}}{(\delta t_s)_{\text{cond.}}} \simeq \frac{|\tau_s|}{T_p(1 - \eta)} = \frac{|\tau_s \tau_i^\pm|}{T_p |\tau_i^\pm - \tau_s|} \gg 1 \quad (51)$$

for $T_p \ll |\tau_s|$. Also in this case the ratio in Eq.(51) can be considered an estimate of the number of entangled modes, and indeed reproduces the asymptotic behaviour of the Schmidt number in Eq.(39).

Following the above arguments, in particular the results (50) and (51), there is no chance that the state become separable when $\tau_s \simeq \tau_i^\pm$, i.e. $\Delta\tau \simeq 0$. When the two photons propagate in the same direction at similar velocities, in fact, detection of one photon will always provide an extremely precise information about the arrival time of the other, basically because they exit the crystal almost simultaneously. This is the typical situation that occurs in the co-propagating case, in the absence of any velocity matching strategy, and explains why co-propagating photons in general display high temporal entanglement.

Conversely, in the counterpropagating geometry the exit times of the twins lack simultaneity because they propagate in opposite directions, and this case is naturally characterized by a strong asymmetry between the twins, in particular they have very different delays $\tau_i^+ \gg |\tau_s|$ from the pump. Because of that, the separable limit (26) can be always realized for intermediate pump durations $\tau_i^+ \gg T_p \gg |\tau_s|$ which need not to be ultrashort because τ_i^+ is a long time scale. This limit physically corresponds to a situation where the forward photon (here the signal) always propagate below the pump pulse, but the pump pulse is short enough that the backward photon rapidly separate from it. In these conditions the temporal localization of the pump provides an absolute timing information on the exit time of the signal, as precise ($\sim T_p$) as the information that can be gained by detecting the idler $\sim T_p(1 - \eta) \approx T_p$, and the exit times of the twins appear uncorrelated. An other way of looking at the situation is that the forward photon is locked to the pump so that it cannot provide any information on the point where down-conversion occurred, and by detecting the signal one does not gain any more precise information on the exit time of the backward idler than by not detecting it.

In the co-propagating configuration, the same limit can be reached only by creating a strong asymmetry between the propagation velocities of the two photons relative to the pump $|\tau_s| \ll |\tau_i^-|$, which in practice requires that the

² Notice that $0 < (1 - \eta) \leq 2$, because of Eq.(14)

signal is velocity matched to the pump [6, 8, 9] as in the example (ii). However, in order that the idler separate from the pump pulse along a finite propagation length, the pump pulse must be in this case ultrashort (Fig.2f). As a consequence, as we shall see in the following, the generated twin photons are broadband.

An alternative strategy, which can be realized only in the co-propagating case, is the so-called symmetric velocity matching [6, 14] where $\tau_s = -\tau_i^-$ and $\eta = -1$, as in the example (iii). This condition, which is rather difficult to achieve, requires that one photon propagate faster than the pump while the other is slower, so that they are symmetrically delayed with respect to the pump center. Negative values of η are in general favorable to separability, because in this case $\Delta\tau = |\tau_i^\pm| + |\tau_s| > |\tau_i^\pm|, |\tau_s|$, and twin photons are more simultaneous with the pump than between themselves. In these conditions, a properly localized pump pulse may provide a timing of the exits of the twins more precise than the information that can be inferred from detection of any of them. Focusing e.g on the case $\eta=-1$, when the pump duration T_p approaches $|\tau_i^-| = |\tau_s|$, both photons are still locked under the pump, so they do not provide sufficient information on the point where generation occurred, and on the other side they are no more simultaneous than the pump duration $\Delta\tau = 2|\tau_i^-| > T_p$.³

This configuration produces rather pure photons (see Figs.4(iii) and 2h). However, their purity is rather far from the ideal result $\mathcal{K}_{min} = 1$ predicted by the Gaussian formula (41), which seems rather an artifact of replacing the sinc by a Gaussian. Actually, if one looks at Fig.2h, which corresponds to the minimum of \mathcal{K} for $\eta = -1$, the joint temporal probability exhibits a diamond-like shape, which does not look really separable in its arguments, and indeed $\mathcal{K}_{min} = 1.18$ is slightly higher than in the other two cases. Notice that in contrast the biphoton probability in the spectral domain in Fig.5h has a nearly circular shape which looks much more factorable (actually in this case deviations from factorability are indicated by the sidelobes of the sinc functions) This demonstrates the usefulness of taking the two complementary views in the temporal and spectral domains. Such imperfect separability is a consequence of the sharp boundaries of the nonlinear medium, which are at the origin of the rectangular box function appearing in Eq.(20). Taking the Gaussian approximation (33), this box function is replaced by a smooth Gaussian of the same width, $\text{Rect}\left(\frac{\bar{t}_s - \bar{t}_i}{\Delta\tau}\right) \rightarrow \exp\left(-\frac{(\bar{t}_s - \bar{t}_i)^2}{4\gamma\Delta\tau^2}\right)$, and then the temporal correlation becomes factorable:

$$\phi(\bar{t}_s, \bar{t}_i) \propto \alpha_p \left(\frac{\bar{t}_s + \bar{t}_i}{2}\right) \text{Rect}\left(\frac{\bar{t}_s - \bar{t}_i}{\Delta\tau}\right) \rightarrow e^{-\frac{\bar{t}_s^2 + \bar{t}_i^2}{4\gamma(\Delta\tau)^2}} \quad \text{for } T_p = T_p^{min} = \sqrt{2\gamma}|\tau_i^-| \quad (52)$$

(the same result is obtained by directly Fourier transforming the Gaussian approximation of $\psi(\Omega_s, \Omega_i)$ in Eq.(33)). Notice that the sharp crystal boundaries have less impact on the separability when $|\eta| \ll 1$, as in the examples i) and ii), because of the elongated shape of the temporal correlation (see Fig.2b and f). These effects might be eliminated and the purity of the heralded photons increased by engineering a Gaussian nonlinearity profile of a poled crystal, as demonstrated by Branczyk et al. [13].

V. SPECTRO-TEMPORAL PROPERTIES OF HERALDED PHOTONS

Once assessed the conditions under which pure single heralded photons can be obtained, it is clearly important to study their individual properties in view of their use in quantum communication/metrology protocols (coupling with atoms, interferometry etc.).

For spontaneous PDC, the marginal statistics of individual photons is described by their first order coherence functions. In the temporal domain, for example, these functions are:

$$G_s^{(1)}(t_s, t'_s) = \langle \hat{a}_s^\dagger(t_s) \hat{a}_s(t'_s) \rangle = \int dt_i \phi^*(t_s, t_i) \phi(t'_s, t_i) \quad (53)$$

$$G_i^{(1)}(t_i, t'_i) = \langle \hat{a}_i^\dagger(t_i) \hat{a}_i(t'_i) \rangle = \int dt_s \phi^*(t_s, t_i) \phi(t_s, t'_i) \quad (54)$$

with analogous definitions in the spectral domain. In terms of its temporal $G^{(1)}$, the reduced state of the heralded photon takes the form

$$\begin{aligned} \hat{\rho}_j &= \frac{1}{\mathcal{N}} \int dt \int dt' G_j^{(1)}(t', t) \hat{a}_j^\dagger(t) |0\rangle \langle 0| \hat{a}_j(t') \\ &= \frac{1}{\mathcal{N}} \int dt \int dt' G_j^{(1)}(t', t) |t\rangle_j \langle t'| \end{aligned} \quad (55)$$

³ Quantitatively, when the pump duration approaches $|\tau_i^\pm|$ in Eq. (50), or $|\tau_s|$ in Eq. (50), then the ratio $\frac{(\delta t_s)_{uncond.}}{(\delta t_s)_{\bar{t}_i}} \rightarrow \frac{1}{1+|\eta|} < 1$.

which in general represents a mixed state, unless the coherence function $G_j^{(1)}(t, t')$ is factorable in its arguments. For equal times, $G_j^{(1)}(t, t) = \langle \hat{A}_j^{\dagger \text{out}}(t) \hat{A}_j^{\text{out}}(t) \rangle = \mathcal{I}_j(t)$ gives the temporal intensity profile of the j-th wave, i.e. the probability distribution of detecting the photon at time t at the crystal exit face. The spectral distribution of the heralded photon can be instead obtained via

$$S_j(\Omega) = \langle \hat{A}_j^{\dagger \text{out}}(\Omega) \hat{A}_j^{\text{out}}(\Omega) \rangle = \int \frac{dt dt'}{2\pi} e^{i\Omega(t-t')} G_j^{(1)}(t, t') \quad (56)$$

For the sake of brevity we limit our analysis to the cases of A) long pump pulses, where the state is highly entangled, and B) conditions where nearly separable states can be realized.

A. Long pump pulses, high entanglement

According to the previous results, when $T_p \gg |\tau_i^\pm| \geq |\tau_s|$ the two-photon state is highly entangled in any configuration. We can for example use the asymptotic form (24) of the joint temporal amplitude(20), and insert it into formulas (53,54). The coherence functions of the signal and the idler obtained in this way are identical (a part from negligible offsets), and have the form

$$G_s^{(1)}(t, t') = G_i^{(1)}(t, t') \rightarrow \frac{g^2}{2\Delta\tau} |\alpha_p(t)|^2 \text{T} \left(\frac{t' - t}{2\Delta\tau} \right) \quad (57)$$

where $\Delta\tau = |\tau_i^\pm - \tau_s|$, and

$$\text{T} \left(\frac{\delta t}{2\Delta\tau} \right) = \begin{cases} 1 - \frac{|\delta t|}{2\Delta\tau} & \delta t \in (-2\Delta\tau, +2\Delta\tau) \\ 0 & \text{elsewhere} \end{cases} \quad (58)$$

is the triangular function, which has the shape of a triangle of base $4\Delta\tau$ and unitary height. This result is the generalization of formula (46) in Ref.[22]. Actually, it holds for any PDC configuration provided that the bandwidths in play are not too broad, because it makes only use of the linear approximations (9) and (15). It shows that when the pump pulse is much longer than the two characteristic time scales, the twin photons have identical properties. The width $\Delta\tau$ of $G^{(1)}(t, t')$ as a function of the time difference $t' - t$ is their *coherence time*, which in this limit is equal to their mutual correlation time [see Eq. (43)]. Conversely, the temporal distributions of twin photons follow the profile of the much longer pump pulse:

$$\mathcal{I}_s(t) = \mathcal{I}_i(t) = \frac{g^2}{2\Delta\tau} |\alpha_p(t)|^2 \quad (59)$$

Notice that from the point of view of classical statistics of light, this behaviour of the $G^{(1)}$, with the peak at $t = t'$ much narrower of the intensity distribution is typical of multimode incoherent light. On the other hand, in the quantum description, the state of the heralded photon in Eq. (55) is in this case mixed, because $G_j^{(1)}(t, t')$ in Eq.(57) is not factorable in its arguments.

The spectra of the photons have the usual sinc² shape characteristic of spontaneous processes

$$S_s(\Omega) = S_i(\Omega) = \frac{g^2}{\sqrt{4\pi}} T_p \text{sinc}^2(\Omega\Delta\tau), \quad (60)$$

and their spectral bandwidths $\Delta\Omega_j = \frac{1}{\Delta\tau}$ are the inverse of the correlation-coherence times. Clearly, this explains why counterpropagating twin-photons are narrowband (order 10 GHz), while co-propagating twin-photons are in general broadband (order THz or more)

B. Nearly separable regime

We start from the case $\eta \ll 1$, including both the counter-propagating and the co-propagating case with asymmetric group velocity matching. We remind that for a pump pulse intermediate between the two time scales $|\tau_i^\pm| \gg T_p \gg |\tau_s|$, one photon propagates locked under the pump while the other separates from it after being generated. For this reason

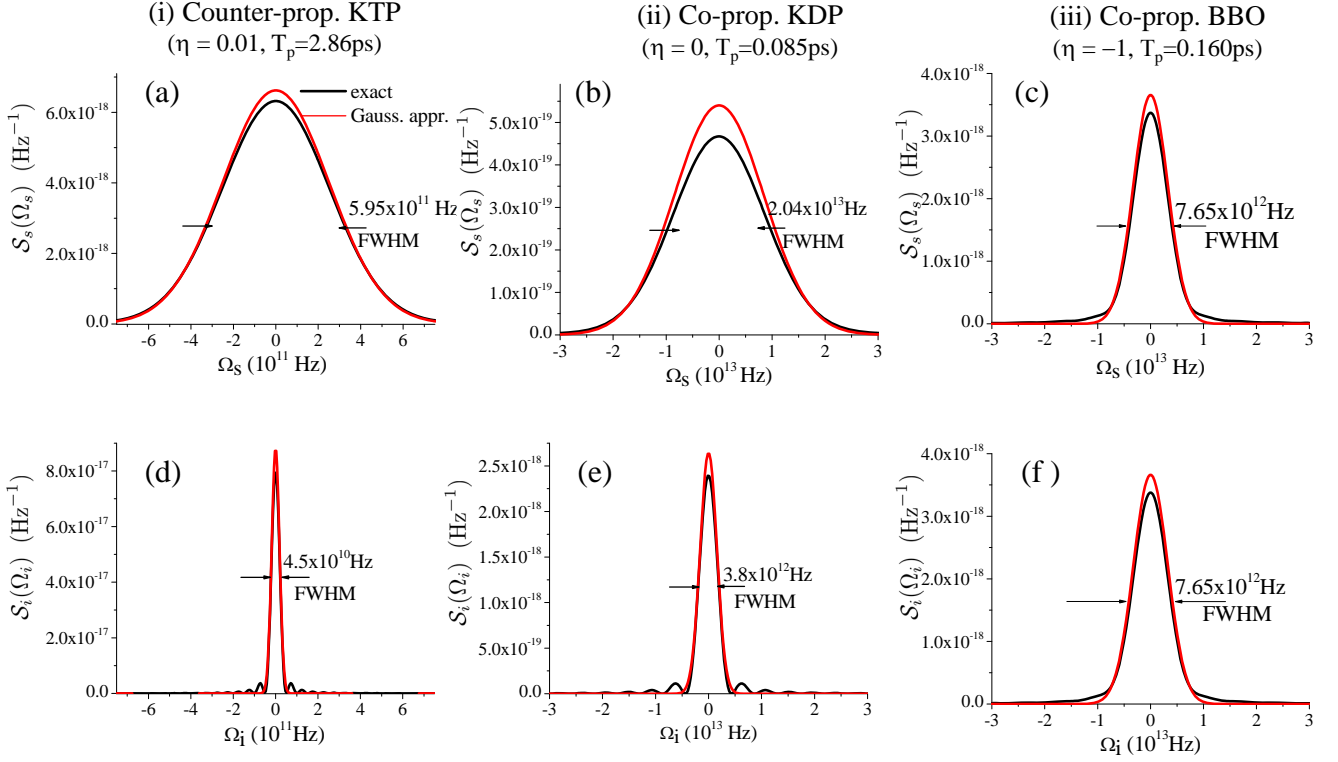


FIG. 6. Spectra of the signal (top) and of the idler (bottom) for the three examples considered in Table I, calculated in conditions of separability of the state, corresponding to panels (b), (f), and (h) of Fig.5. Black lines: exact numerical results. Red lines: Gaussian approximated ones. Notice in column (i) and (ii) the Gaussian profiles of the signal and the narrower sinc² profiles of the idler spectra as predicted by Eq.(63) and (66).

the properties of the two photons are strongly asymmetric, as e.g. shown by the spectra in column (i) and (ii) of Fig.6. By using the asymptotic limit(26) of the joint temporal amplitude, and inserting it into formulas (53,54), we obtain for the signal photon:

$$G_s^{(1)}(\bar{t}_s, \bar{t}'_s) = \frac{g^2}{2\Delta\tau} \alpha_p^*(\bar{t}_s) \alpha_p(\bar{t}'_s) \quad (61)$$

which implies that

$$\mathcal{I}_s(t) = \frac{g^2}{2\Delta\tau} |\alpha_p(t - t_{As})|^2, \quad (62)$$

$$S_s(\Omega) = \frac{g^2}{2\Delta\tau} |\tilde{\alpha}_p(\Omega)|^2 \quad (63)$$

i.e. the photon that propagates locked under the pump entirely inherits the spectro-temporal properties of the coherent pump laser.

Conversely for the idler photon

$$G_i^{(1)}(t, t') = \frac{g^2}{2\Delta\tau} \frac{\sqrt{\pi} T_p}{2\Delta\tau} \text{Rect}\left(\frac{\bar{t}_i}{\Delta\tau}\right) \text{Rect}\left(\frac{\bar{t}'_i}{\Delta\tau}\right), \quad (64)$$

and its properties depend on the dispersion properties of the crystal and on its length, through the parameter $\Delta\tau = |\tau_i^\pm - \tau_s|$. In particular

$$\mathcal{I}_i(t) = \frac{g^2}{2\Delta\tau} \frac{\sqrt{\pi} T_p}{2\Delta\tau} \text{Rect}\left(\frac{t - t_{Ai}}{\Delta\tau}\right), \quad (65)$$

$$S_i(\Omega) = \frac{g^2}{\sqrt{4\pi}} T_p \text{sinc}^2(\Omega\Delta\tau), \quad (66)$$

The temporal distribution of the idler photon is a rectangular pulse of duration $2\Delta\tau$, because for such a short pump the idler photon distribution reflect simply the fact that it can be generated anywhere in the crystal with uniform probability. Remarkably, since $\Delta\tau \simeq |\tau_i^\pm| \gg T_p$, the idler wavepacket has a longer duration than the pump itself. In particular, in the counterpropagating case, its duration roughly corresponds to the transit time of the pump along the crystal. The idler spectrum retains the same sinc² shape as in the long pump limit, with a bandwidth $\Delta\Omega_i = 1/\Delta\tau \ll \Delta\Omega_p$. Hence, when the state is approximately separable, the heralded idler photon is not only pure, but also more monochromatic than the pump laser that drives the process. However, only in the case (a) this result really means that the generated idler photon is narrowband, as shown by figure 6d, while in case b) it is anyway quite broadband (see Fig.6e), because separability requires ultra-broadband pump pulses. Interestingly, in the counterpropagating case the strong asymmetry between the twin photons, and the fact that the idler is more monochromatic than the pump, reflect the unusual coherence properties of the classical signal and idler field generated above the MOPO threshold, described in [34, 35].

The forms of the coherence functions of the signal and idler, $G^{(1)}(t, t') = \sqrt{\mathcal{I}(t)}\sqrt{\mathcal{I}(t')}$, is typical of single-mode light, which possess classical temporal coherence: indeed it means that the average length of a temporal fluctuation (the coherence time) is equal to the duration of the wave-packet, implying that the statistics is a sort of frozen in time. In the quantum description the states of the heralded signal and idler photon are pure $\hat{\rho}_j = |\psi_j\rangle\langle\psi_j|$, with

$$|\psi_s\rangle = \frac{1}{(\sqrt{\pi}T_p)^{1/2}} \int dt_s \alpha_p(t_s - t_{A_s}) \hat{a}_s^\dagger(t_s)|0\rangle \quad (67)$$

$$|\psi_i\rangle = \frac{1}{\sqrt{2\Delta\tau}} \int dt_i \text{Rect}\left(\frac{t_i - t_{A_i}}{\Delta\tau}\right) \hat{a}_i^\dagger(t_i)|0\rangle \quad (68)$$

Finally we consider the alternative technique for reaching separability, i.e. the configuration with $\tau_s = -\tau_i$ ($\eta = -1$), in which the two photons co-propagate symmetrically delayed with respect to the pump center. As can be intuitively understood, in this case the properties of the twin photons are completely symmetric. The mere linear approximation does not give particularly expressive results, so that we have to resort to the stronger Gaussian approximation. According to it, separability is reached at $T_p = T_p^{\text{min}} = \sqrt{2\gamma}|\tau_i^-|$, where (calculations not reported here) the state of each heralded photon becomes pure, $G_j^{(1)}(t, t') = \sqrt{\mathcal{I}_j(t)}\sqrt{\mathcal{I}_j(t')}$, with the temporal and spectral distributions of the two waves given by

$$\mathcal{I}_s(\bar{t}_s) = \mathcal{I}_i(\bar{t}_i) \propto e^{-\frac{(t-t_{A_j})^2}{2T_p^2}} = |\alpha_p\left(\frac{\bar{t}_j}{\sqrt{2}}\right)|^2 \quad (69)$$

$$S_s(\Omega) = S_i(\Omega) \propto |\alpha_p(\sqrt{2}\Omega)|^2 \quad (70)$$

i.e. the two waves have similar properties as the pump, but with a slightly longer duration and a slightly narrower spectrum. As shown by panel (iii) of Fig.6, these Gaussian results are rather close to the exact ones.

C. Mean number of down-converted pairs-Efficiency

An other important point in view of applications is the efficiency by which heralded pure photons can be generated. In the separable regime, where the state is approximately single-mode, this ultimately depends on the probability that a photon pair is generated by a pump pulse crossing the crystal ⁴ For a given pump energy and crystal length, we shall see that the symmetric case $\eta = -1$ is much more efficient than the asymmetric case $|\eta| \ll 1$: this is quite natural because in the first case both photons propagate close to the pump, while in the latter case one photonic wavepacket rapidly separates from it, so that the effective interaction length is strongly reduced.

The probability of generating at least a photon pair can be easily calculated from the state (5) as $\frac{\mathcal{N}}{1+\mathcal{N}} \approx \mathcal{N}$ for $\mathcal{N} \ll 1$, where \mathcal{N} is the mean number of photon pairs per pulse. Within the linear approximation, making e.g. use of Eq. (20) we obtain

$$\mathcal{N} = \int dt_s \int dt_i |\phi(t_s, t_i)|^2 = g^2 \frac{\sqrt{\pi}T_p}{2\Delta\tau} \quad (71)$$

⁴ We are assuming an ideal unit efficiency of detection

Notice that this formula is valid for any geometry and any value of T_p (of course, provided that $\Delta\tau \neq 0$). However, the number of down-converted pairs may be quite different in different regimes.

In the long-pump regime, where the state is highly entangled, the number of down-converted photons is approximately

$$\mathcal{N} \simeq \frac{g^2}{2} \mathcal{K} \gg g^2, \quad (72)$$

where we used the asymptotic expression of the Gaussian Schmidt number in Eq.(38). Roughly speaking, the number of photon pairs is the number of photons per mode that one would have in the strictly CW pump regime, multiplied by the number of entangled modes \mathcal{K} .

Let us then consider the separable regimes. In the symmetric case $\eta = -1$,

$$\mathcal{N} = \frac{g^2}{4} \frac{\sqrt{\pi} T_p}{|\tau_i^\pm|} \approx \frac{g^2}{4} \sqrt{2\pi\gamma} \quad (73)$$

where in the last expression we inserted the Gaussian value of the pump duration (40) $T_p^{min} = \sqrt{2\gamma|\tau_s\tau_i^\pm|}$ at which the best separability is achieved. Considering that $\sqrt{2\pi\gamma} \approx 1$, then the mean number of down-converted photons is close to $g^2/4$.

In the asymmetric case $\eta \ll 1$ (counterpropagating or co-propagating case with asymmetric group-velocity matching), instead

$$\mathcal{N} = \frac{g^2}{2} \frac{\sqrt{\pi} T_p}{(1-\eta)|\tau_i^\pm|} \simeq \frac{g^2}{2} \frac{\sqrt{\pi} T_p}{|\tau_i^\pm|} \ll \frac{g^2}{2} \quad (74)$$

because separability is achieved for $T_p \ll |\tau_i^\pm|$.⁵ Notice that in this latter case the efficiency is strongly reduced, because of the lack of superposition between the pump and the idler wave. We remind that this configuration is characterized by the fact that the idler wavepacket rapidly separates from the short pump pulse $T_p \ll |\tau_i^\pm|$. Since $g \propto l_c$ it effectively works as if the crystal length were reduced to a shorter length

$$l_c \longrightarrow l_c \sqrt{\frac{T_p}{|\tau_i^\pm|}}. \quad (75)$$

At this point one is naturally lead to wonder whether filtering the spectral or temporal modes would not lead to the same or better efficiency. If a long enough pump pulse is used, the number of photon pairs goes as $\simeq \mathcal{K} \frac{g^2}{2}$. Let us then suppose that it is possible to make a "clever" filtering, which projects the state onto a single Schmidt mode: even assuming that all the Schmidt modes have the same weight, a fraction $1/\mathcal{K}$ of the total number of modes would then be transmitted, leading to $\mathcal{N} = \frac{g^2}{2}$, which is anyway better than what could be obtained with asymmetric group-velocity matching. However, practical considerations, which are outside the scope of this theoretical work, may then lead to conclude that it is anyway better to directly generate a factorable state

VI. SUMMARY AND CONCLUSIONS

In this work we compared different phase-matching configurations which are known to generate pure heralded single photons from spontaneous parametric down-conversion, namely the counter-propagating configuration, and the co-propagating configuration with asymmetric and symmetric group velocity matching. We provided a systematic analysis of the conditions under which uncorrelated twin photons can be generated, which basically hold for any PDC configuration, provided that the bandwidth in play are not too broad. In our description all the properties of the source are condensed in two time scales τ_s, τ_i^\pm characteristic of the relative propagation of the three waves inside the medium.

On the one side, we performed a sort of standard analysis in the spectral domain, where we derived a simple formula for the Schmidt number of entanglement, that permits to evaluate the degree of purity of the heralded photons via a single parameter. On the other side, the less standard analysis of the correlation of twin photons in the temporal domain clarifies in a more physical sense the role of the two characteristic time scales, and permits to understand the mechanism under which the temporal correlation between twin photons can be eliminated. In particular it shows

⁵ If we use the Gaussian result for T_p^{min} , we also can write $N \approx \frac{g^2}{2} \sqrt{|\eta|}$.

that one way of eliminating this temporal correlation relies on creating a strong asymmetry between the velocities of the two down-converted waves relative to the pump wave, so that one photon propagates locked under the pump while the other, for a pump pulse sufficiently localized inside the crystal, separates from it. In this conditions, the timing provided by the pump pulse may be more precise than that offered by detecting any of the twin photons, and the arrival times of the two photons appear uncorrelated. Such an asymmetry in the relative propagation velocities is naturally present in the counter-propagating geometry, because of the natural separation of the GVM and the GVS time scales, but requires particular tuning conditions in the co-propagating geometry. Because of this unique feature, counter-propagating twin photons in a pure state can in principle be heralded at any frequency by choosing the required poling period. Moreover, the twin photons are naturally narrow-band, especially the one propagating opposite to the pump direction, and separability is achieved for a broad range of pump pulse durations.

An other way of eliminating the correlation, which can be implemented only for co-propagating photons, requires that the twin photons propagate symmetrically delayed with respect to the pump pulse. Also in this case our analysis shows that in proper conditions the timing information which can be gained from a localized pump can be better than from any of the twins, but the required pump duration is ultrashort, and the generated twins are broadband. Although the purity of heralded photons generated in this way appears somehow lower, symmetric group velocity matching has the advantage of a higher efficiency of pair production, because both twin photons propagate close to the pump. Conversely, the asymmetric group-velocity matching and the counterpropagating geometry are characterized by a low efficiency, because purity requires that one photonic wavepacket separates from the pump pulse, so that the effective interaction length is reduced.

In conclusion we provided a systematic study of the generation of pure heralded single-photons through spontaneous PDC, which may turn useful for optimizing the existing configurations in view of different applications. For example when narrowband single-photons are required, the counter-propagating configuration is the natural choice. In addition, once the technical challenges for the fabrication of crystals with sub-micrometer poling periods are overcome, this strategy offers more flexibility since it can be virtually implemented for any wavelength, and generates pure single-photons for a broad range of pump durations. In contrast, twin photons emitted in the common co-propagating geometry are naturally broadband and can be generated in a separable state only for very short pulses, under particular tuning conditions. Thus this is the good choice when broadband photons and or high repetition rates are required. Finally, if efficiency is the main issue, the symmetric group velocity matching should represent the best choice. We also hope that our general analysis, by providing a deeper and more intuitive understanding of the mechanism through which the temporal entanglement of twin photons can be eliminated, may stimulate new strategies of heralded photon generation.

Appendix A: Specific configurations

According to the results presented Sec. II and III, we considered three configurations suitable for generating pure heralded photons, and a specific example for each configurations :

(i) Counter-propagating geometry ($|\eta| \ll 1$)

The peculiarity of the counter-propagating geometry is that the condition $|\eta| \ll 1$ is naturally fulfilled, so that any phase-matching configuration has the potentiality to generate pure heralded photons. As a specific example, we considered a 10mm long periodically poled crystal of Potassium Titanyl Phosphate (PPKTP) in a type 0 (e-ee) phase-matching configuration: the poling period is $\Lambda = 800\text{nm}$, $\lambda_p = 814.5\text{nm}$, $\lambda_s = 1145\text{nm}$, $\lambda_i = 2932.4\text{nm}$, $\eta = \tau_s/\tau_i^+ = 0.01$. Apart from the length of the crystal, the parameters are those of the experiment reported in [17]), and are not particularly optimized for separability. Notice that for the same crystal, the condition $\eta = 0$ can be also realized, and would lead to a higher degree of purity, as discussed in Ref.[1].

For the co-propagating geometry we considered two examples of asymmetric $\eta = 0$ and symmetric group velocity matching ($\eta = -1$), taken from the literature [6–9], in particular the example (II) is that of the experiment by Mosley et al. [8].

(ii) Co-propagating geometry, asymmetric group velocity matching $\eta = 0$

We considered a 10mm Potassium Dihydrogen Phosphate (KDP) crystal cut for type II collinear phase-matching (e-oe) at degeneracy. When pumped at 415nm with a tuning angle $\theta_p = 68.7^\circ$ with the crystal axis, the KDP crystal has the peculiarity of displaying a vanishing GVM between pump and the signal field (i.e. $\tau_s = 0$, $\eta = 0$) and is therefore well suited for the generation a separable two-photon state provided that $T_p \ll \tau_i^- = 0.72\text{ps}$ [6, 9].

(iii) Co-propagating geometry, symmetric group velocity matching $\eta = -1$

The symmetric condition $\eta = -1$ can be fulfilled only in the co-propagating configuration, and is rather difficult to meet because it requires that the pump inverse group velocity falls exactly midway between the signal and the idler

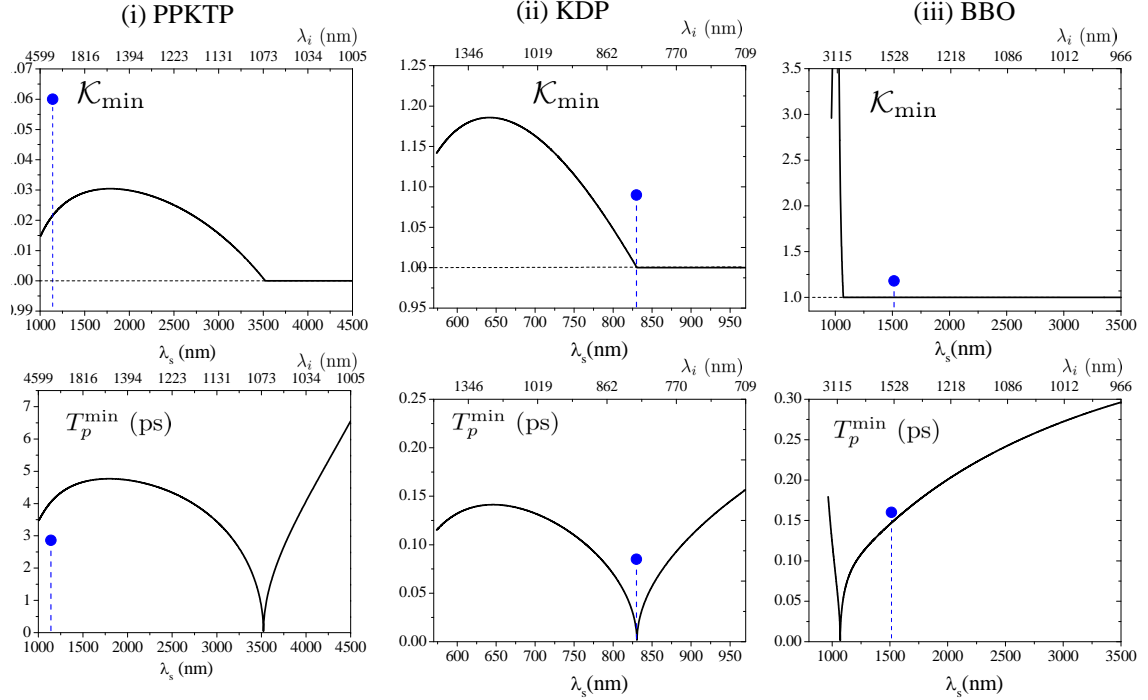


FIG. 7. Minimum of the Schmidt number K_{min} (top panels) and relative pump duration T_p^{min} (bottom panels) as a function of the signal wavelength, evaluated with the Gaussian approximation in Eqs.(41) and (40), for the three crystals in Table I. The blue dots are the value numerically calculated at the minima of \mathcal{K} in Fig.4, and correspond to the parameters of Fig. 2(b) (f) and (h). The top horizontal scale shows the conjugate idler wavelength λ_i .

inverse group velocities

$$\tau_i^- = -\tau_s \longleftrightarrow \frac{1}{2} \left(\frac{1}{v_{gs}} + \frac{1}{v_{gi}} \right) = \frac{1}{v_{gp}} \quad (\text{A1})$$

Provided this relation is satisfied, the two-photon correlation $\psi(\Omega_s, \Omega_i)$ in the Gaussian approximation displays a circular shape for $T_p = T_p^{min}$, since $c_{12} = 0$ and $c_{11} = c_{22} = 2\gamma\tau_s^2$. For the optimized pump pulse duration, the generated twin photons are thus not only uncorrelated but also indistinguishable.

As a specific example we considered a 10mm Beta-Barium Triborate (BBO) crystal both cut for type II collinear phase-matching (e-oe) at degeneracy. When pumped at 757nm with a pump tuning angle $\theta_p = 28.8^\circ$ the condition $\tau_s = -\tau_i^+ = 0.237ps$, $\eta = -1$ is realized.

Table I summarizes the parameters for three examples chosen as representative of the configurations (i), (ii) and (iii).

Fig. 7 plots the results of the Gaussian approximation for K_{min} and T_p^{min} [Eqs. (41) and (40)], as a function of the signal central wavelengths λ_s , for these three examples. The phase-matched wavelengths, λ_s and λ_i , and the corresponding characteristic times τ_s and τ_i^\pm are evaluated using the Sellmeier dispersion formula reported in [26–28]. For the PPKTP crystal, different wavelengths corresponds to different poling periods Λ , not reported in the figure. For the bulk KDP and BBO crystals the signal and idler central wavelengths are varied by changing the tuning angle θ_p between the pump direction and the crystal axis (not reported in the figure). Notice that in the BBO case η is always negative for $\lambda_s > 1070$ nm, so that the generated two-photon state is separable when the crystal is tuned on those wavelengths according to approximation (41). Notice also that for $\lambda_s = 1010$ nm the group velocities of the signal and idler fields becomes equal ($\eta = 1$) and the Schmidt number predicted by Eq.(37) goes to infinity. Under these conditions the SPDC bandwidths and the number entangled modes are in fact very large, through not infinite, as they are only limited by group-velocity dispersion, a feature not taken into account in the simplified model based the linearized propagation (9) (15).

-
- [1] A. Gatti, T. Corti, and E. Brambilla, *Phys. Rev. A* **92**, 053809 (2015).
- [2] M. Eisaman, J. Fan, M. A., and S. V. Polyakov, *Review of Scientific Instruments* **82**, 071101.
- [3] A. Migdall, S. Polyakov, J. Fan, and J. Bienfang, eds., *Single-Photon Generation and Detection: Physics and Applications*, Experimental Methods in the Physical Sciences, Vol. 45 (Academic Press, 2013).
- [4] A. Christ, A. Fedrizzi, H. Hbel, T. Jennewein, and C. Silberhorn, in *Single-Photon Generation and Detection Physics and Applications*, Experimental Methods in the Physical Sciences, Vol. 45, edited by J. F. Alan Migdall, Sergey V. Polyakov and J. C. Bienfang (Academic Press, 2013) Chap. 11, pp. 351 – 410.
- [5] A. McMillan, Y.-P. Huang, B. Bell, A. Clark, P. Kumar, and J. Rarity, in *Single-Photon Generation and Detection Physics and Applications*, Experimental Methods in the Physical Sciences, Vol. 45, edited by J. F. Alan Migdall, Sergey V. Polyakov and J. C. Bienfang (Academic Press, 2013) pp. 411 – 465.
- [6] W. P. Grice, A. B. U'Ren, and I. A. Walmsley, *Phys. Rev. A* **64**, 063815 (2001).
- [7] A. B. U'Ren, C. Silberhorn, K. Banaszek, I. A. Walmsley, R. Erdmann, W. P. Grice, and M. G. Raymer, *Laser Physics* **15**, 146161 (2006).
- [8] P. J. Mosley, J. S. Lundeen, B. J. Smith, P. Wasylczyk, A. B. U'Ren, C. Silberhorn, and I. A. Walmsley, *Phys. Rev. Lett.* **100**, 133601 (2008).
- [9] P. J. Mosley, J. S. Lundeen, B. J. Smith, and I. A. Walmsley, *New Journal of Physics* **10**, 093011 (2008).
- [10] A. L. Migdall, D. Branning, and S. Castelletto, *Phys. Rev. A* **66**, 053805 (2002).
- [11] Z. H. Levine, J. Fan, J. Chen, A. Ling, and A. Migdall, *Opt. Express* **18**, 3708 (2010).
- [12] R. S. Bennink, *Phys. Rev. A* **81**, 053805 (2010).
- [13] A. M. Brańczyk, A. Fedrizzi, T. M. Stace, T. C. Ralph, and A. G. White, *Opt. Express* **19**, 55 (2011).
- [14] L. Zhang, C. Soeller, O. Cohen, B. J. Smith, and I. A. Walmsley, *J. of Mod. Optics* **59**, 1525 (2012).
- [15] A. Christ, A. Eckstein, P. J. Mosley, and C. Silberhorn, *Opt. Expr.* **17**, 3441 (2009).
- [16] S. E. Harris, *Appl. Phys. Lett.* **9**, 114 (1966).
- [17] C. Canalias and V. Pasiskevicius, *Nat. Photon.* **1**, 459 (2007).
- [18] C. Canalias, V. Pasiskevicius, R. Clemens, and F. Laurell, *Appl. Phys. Lett.* **82**, 4233 (2003).
- [19] V. Pasiskevicius, G. Strmqvist, F. Laurell, and C. Canalias, *Opt. Materials* **34**, 513 (2012).
- [20] G. Strmqvist, V. Pasiskevicius, C. Canalias, P. Aschieri, A. Picozzi, and C. Montes, *J. Opt. Soc. Am. B* **29**, 1194 (2012).
- [21] T. Suhara and M. Ohno, *IEEE Journal of Quantum Electronics* **46**, 1739 (2010).
- [22] T. Corti, E. Brambilla, and A. Gatti, *Phys. Rev. A* **93**, 023837 (2016).
- [23] A. Gatti, T. Corti, and E. Brambilla, *ArXiv e-prints arXiv:1704*.
- [24] J. Monroy-Ruz, K. Garay-Palmett, and A. B. U'Ren, *New Journal of Physics* **18**, 103026 (2016).
- [25] P. G. Evans, R. S. Bennink, W. P. Grice, T. S. Humble, and J. Schaake, *Phys. Rev. Lett.* **105**, 253601 (2010).
- [26] G. G. Gurzadian, V. G. Dmitriev, and D. N. Nikogosian, *Handbook of nonlinear optical crystals* (Springer-Verlag Berlin, New York, 1991).
- [27] K. Kato and E. Takaoka, *Appl. Opt.* **41**, 5040 (2002).
- [28] F. Zernike, *J. Opt. Soc. Am.* **54**, 1215 (1964).
- [29] A. Ekert and P. L. Knight, *American Journal of Physics* **63**, 415 (1995).
- [30] S. Parker, S. Bose, and M. B. Plenio, *Phys. Rev. A* **61**, 032305 (2000).
- [31] M. P. van Exter, A. Aiello, S. S. R. Oemrawsingh, G. Nienhuis, and J. P. Woerdman, *Phys. Rev. A* **74**, 012309 (2006).
- [32] A. Gatti, T. Corti, E. Brambilla, and D. B. Horoshko, *Phys. Rev. A* **86**, 053803 (2012).
- [33] Y. M. Mikhailova, P. A. Volkov, and M. V. Fedorov, *Phys. Rev. A* **78**, 062327 (2008).
- [34] G. Strmqvist, V. Pasiskevicius, C. Canalias, and C. Montes, *Phys. Rev. A* **84**, 023825 (2011).
- [35] C. Montes, B. Gay-Para, M. D. Micheli, and P. Aschieri, *J. Opt. Soc. Am. B* **31**, 3186 (2014).